

Strength of Brittle Materials under High Strain Rates in DEM Simulations

Jorge Daniel Riera¹, Leticia Fleck Fadel Miguel² and Ignacio Iturrioz³

Abstract: In the truss-like Discrete Element Method (DEM), masses are considered lumped at nodal points and interconnected by means of uni-dimensional elements with arbitrary constitutive relations. In previous studies of the tensile fracture behavior of concrete cubic samples, it was verified that numerical predictions of fracture of non-homogeneous materials using DEM models are feasible and yield results that are consistent with the experimental evidence so far available. Applications that demand the use of large elements, in which extensive cracking within the elements of the model may be expected, require the consideration of the increase with size of the fractured area, in addition to the effective stress-strain curve for the element. This is a basic requirement in order to achieve mesh objectivity. Note that the degree of damage localization must be known *a priori*, which is a still unresolved difficulty of the non-linear fracture analysis of non-homogeneous large structures. In previous DEM applications, the authors have noticed that simulations conducted on samples of fragile, inhomogeneous materials subjected to various loading conditions, tend to fail under increasing loads when the loading rate increases. The issue raised questions, such as the need to explain the capacity of the method to predict, at least approximately, the increase in load-carrying capacity of structural systems subjected to impact and blast loadings, the need to assess the correlation with experimental results and to critically examine the validity of the available experimental evidence. Within this context, this paper presents the response of cubic concrete samples subjected to tension under controlled boundary displacements with increasing loading rates, obtained by simulation with the DEM. Next DEM simulations of modified Hopkinson bar tests are presented with the aim of extending the range of strain rates examined. Conclusions on model uncertainty associated to high strain or loading rates, as well as theoretical considerations on the applicability of available experimental results are finally advanced.

¹ Department of Civil Engineering, UFRGS, Porto Alegre, Brazil. jorge.riera@ufrgs.br

² Department of Mechanical Engineering, UFRGS, Porto Alegre, Brazil. letffin@ufrgs.br

³ Department of Mechanical Eng., UFRGS, Porto Alegre, Brazil. ignacio@mecanica.ufrgs.br

Keywords: Tensile Strength, Rate Effects, High Strain Rates, Fracture, Concrete, Inhomogeneous Materials, Discrete Element Method.

1 Introduction

Predicting the response up to failure of solids subjected to dynamic loads, in particular post-peak response, employing methods based on Continuum Mechanics present disadvantages in comparison with discrete models of the solids under consideration. This is a consequence of material fracture, which introduces discontinuities in the displacement functions that are difficult to handle in a continuum formulation and fostered the rapid development of more efficient methods of analysis. Among various such methods, the so-called truss-like Discrete Element Method (DEM) proves quite appealing. The approach was proposed by Riera (1984) to determine the dynamic response of plates and shells under impact loading when failure occurs primarily by tension, which is generally the case in concrete structures. The lack of sufficient experimental evidence in this area to confirm DEM predictions, led to the assessment of its performance in structures subjected to quasi-static loading.

The response of geometrically similar reinforced concrete beams built in four different sizes was determined numerically to quantify size effects in reinforced concrete beams (Rios and Riera, 2004). The inhomogeneous character of concrete was accounted for by assuming that the specific fracture energy is a random field in 3D-space, while the constitutive criteria was based on Hillerborg's model (1971). The discrete numerical model was also used to reproduce experimental results due to van Vliet and van Mier (2000) on the influence of sample size on the tensile strength of concrete and rock as well as the strength of large rock dowels subjected to shear (Miguel *et al.*, 2008).

In response determinations of structures with initial cracks or high stress gradients, which result in fracture localization, well established procedures lead to results that are mesh independent. However, in elements subjected to approximately uniform stress fields a hitherto unknown problem arises in the analysis of non-homogeneous materials: the need to know *a priori* the degree of fracturing of the element. This also affects finite element analysis in cases in which there is no clear fracture localization, requiring a careful evaluation of the energy dissipated by fracture or other mechanisms in the course of the loading process (Miguel *et al.*, 2010). Tentative criteria to account for the effect in non-linear dynamic fracture analysis of large structural systems were proposed by Riera *et al.* (2008).

In addition, under impact, blast and other short duration loadings, it has long been acknowledged that the strength of engineering materials tends to increase with the

loading (or strain) rate. In DEM applications, the authors have noticed that simulations conducted on samples of fragile, inhomogeneous materials subjected to various loading conditions, tend to fail under increasing loads when the loading rate increases. This phenomenon was observed for exactly the same simulated samples, assuming rate-independent material properties, under the same boundary conditions: only the rate of loading was altered. The issue raised a number of questions, such as the need to explain the capacity of the DEM to predict, at least approximately, the increase typically observed in load-carrying capacity of structural systems subjected to impact and blast loadings, the need to assess the correlation with experimental results under different loading conditions and, last but not least, to critically examine the experimental evidence for very high strain rates available in the technical literature.

With the purpose of clarifying the issues listed above, this paper presents results obtained by simulation with the Discrete Element Method (DEM) on prismatic concrete samples subjected to tension, by analyzing the samples under a set of increasing loading rates. The study leads to predictions of the sample behavior, including the cracking pattern. The failure stresses are compared with experimental results. Similar objectives were pursued by Hentz *et al.* (2004), who employ a 3D discrete element method to determine the response of concrete samples subjected to dynamic loading. The model, which consists of spheres in contact, was previously validated through quasi-static simulations. After performing a quasi-static identification of the model parameters, compressive dynamic tests were first simulated. The model proved capable of reproducing the influence of the strain rate on concrete strength, and confirms the inertia-based hypothesis at high strain rates. However, the dynamic tensile tests simulations led Hentz *et al.* (2004) to argue that a local rate effect has to be introduced to reproduce the experimental rate dependency, which would then be a material-intrinsic effect. Kim and Lim (2011) also present results on rate dependent fracture in concrete using an irregular lattice model, similar to the DEM used in the present paper, while Ozbolt *et al.* (2011) focus on a 3D finite-element study of crack propagation in concrete compact tension specimen. The rate sensitive microplane model is used as a constitutive law for concrete. The results of the study show that the fracture of the specimen strongly depends on the loading rate. For relatively low loading rates there is a single crack due to the mode-I fracture. However, with the increase of loading rate, crack branching is observed. Up to certain threshold (critical) loading rate, the maximum crack velocity increases with increase of the loading rate, while for higher loading rates the peak velocity of crack propagation becomes independent of the loading rate.

2 Experimental evidence

A large body of experimental evidence confirms the contention that the strength of brittle materials, like concrete, increases with the rate of loading. A brief overview of available results will be presented in this section, as well as a summary of models proposed to account for the effect, such as the chemical reaction-rate process theory, stochastic theories and material inertia models. Constitutive models proposed for concrete, such as rheological, porous media and viscoelastic models are also addressed. Figure 1 presents experimental evidence on the influence of the strain-rate on the concrete tensile strengths reported by Malvar and Crawford (1998).

Envelopes of the various experimental observations of the dynamic/static strengths (η) ratio for concrete in uniaxial tension collected by Malvar and Crawford (1998) and Cotsovos and Pavlovic' (2008), jointly with the fit to DEM numerical simulations due to Miguel *et al.* (2012) are shown in Figure 2. Recent test results for concrete loaded at high strain rates in tension, obtained with a new experimental technique based on the Hopkinson bar principle combined with the spalling phenomenon, as well as numerical simulations of those experiments, were presented by Brara *et al.* (2001), Brara and Klepaczko (2007) and Weerheijm and Van Doormaal (2007) and will be discussed in Section 6.

3 The discrete element method (DEM) in fracture problems

The Discrete Element Method employed in this paper is based on the representation of a solid by means of an arrangement of elements able to carry only axial loads. The discrete elements representation of the orthotropic continuum was adopted to solve structural dynamics problems by means of explicit direct numerical integration of the equations of motion, assuming the mass lumped at the nodes. Each node has three degrees of freedom, corresponding to the nodal displacements in the three orthogonal coordinate directions. The equations that relate the properties of the elements to the elastic constants of an isotropic medium are:

$$\delta = \frac{9\nu}{4-8\nu}, \quad EA_n = EL_0^2 \frac{(9+8\delta)}{2(9+12\delta)}, \quad EA_d = \frac{2\sqrt{3}}{3} A_n \quad (1)$$

in which E and ν denote Young's modulus and Poisson's ratio, respectively, while A_n and A_d represent the areas of normal and diagonal elements.

The resulting equations of motion may be written in the well-known form:

$$\mathbf{M}\ddot{\vec{x}} + \mathbf{C}\dot{\vec{x}} + \vec{F}_r(t) - \vec{P}(t) = \vec{0} \quad (2)$$

in which \vec{x} represents the vector of generalized nodal displacements, \mathbf{M} the diagonal mass matrix, \mathbf{C} the damping matrix, also assumed diagonal, $\vec{F}_r(t)$ the vector of

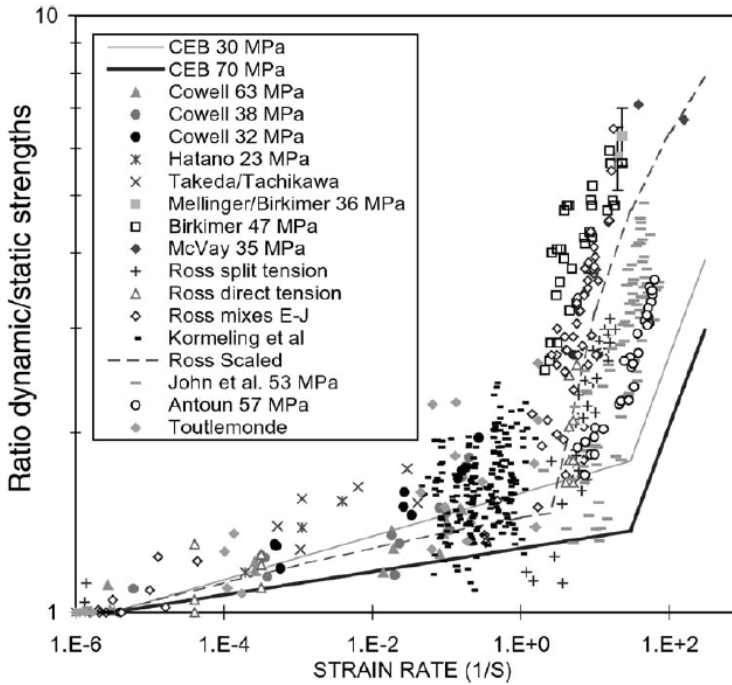


Figure 1: Effect of strain-rate on the tensile strength of concrete (from Malvar and Crawford, 1998).

internal forces acting on the nodal masses and $\vec{P}(t)$ the vector of external forces. Obviously, if \mathbf{M} and \mathbf{C} are diagonal, Equations (2) are not coupled. Then the explicit central finite differences scheme may be used to integrate Equation (2) in the time domain. Since the nodal coordinates are updated at every time step, large displacements can be accounted for in a natural and efficient manner.

In the present paper, the relation between tensile stress and strain in the material proposed by Hillerborg (1971) was adopted. Another important feature of the approach is the assumption that G_f is a 3D random field with a Weibull probability distribution. It should be underlined again that fracture localization weakens as the non-homogeneous nature of the material becomes more pronounced, *i.e.*, as the coefficients of variation of the variables that describe the material properties increase.

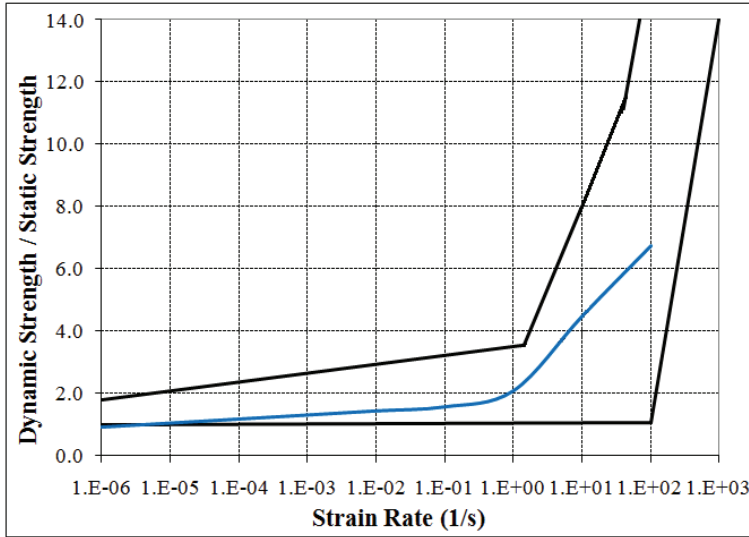


Figure 2: Envelopes of experimental observations of the dynamic/static strengths ratio (η) for concrete in uniaxial tension collected by Malvar and Crawford (1998) and Cotsovos and Pavlovic' (2008) in black lines, and in continuous blue line the DEM prediction (from Miguel *et al.*, 2012).

4 Non-linear constitutive model for material damage

The softening law for quasi fragile materials proposed by Hilleborg (1971) was adopted to handle fragile fracture by means of the triangular constitutive relationship (ECR) shown in Figure 3, which allows accounting for the irreversible effects of crack nucleation and propagation. The area under the force *vs.* strain curve (the area of the triangle OAB in Figure 3) represents the energy density necessary to fracture the area of influence of the element. Thus, for a given point P on the force *vs.* strain curve, the area of the triangle OPC represents the reversible elastic energy density stored in the element, while the area of the triangle OAP is proportional to the energy density dissipated by damage. Once the damage energy density equals the fracture energy, the element fails and loses its load carrying capacity. On the other hand, in the case of compressive loads the material behavior is assumed linearly elastic. Thus, failure in compression is induced by indirect tension.

Constitutive parameters and symbols are shown in Figure 3. The element axial force F depends on the axial strain ϵ . The area associated to each element is given by Equations (6) and (7) for longitudinal and diagonal elements, respectively. An equivalent fracture area A_i^* of each element is defined in order to satisfy the con-

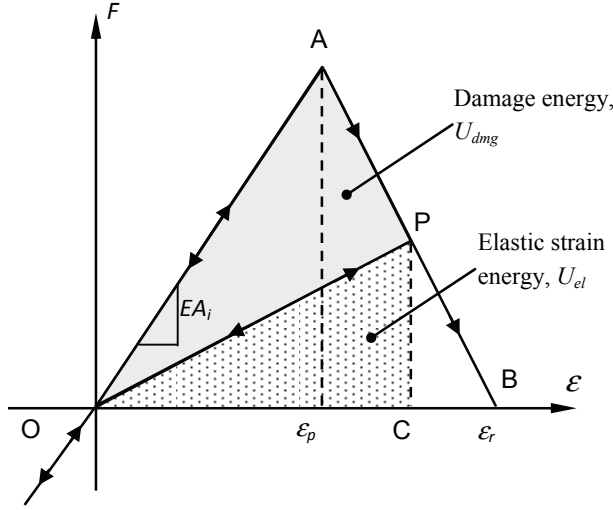


Figure 3: Triangular constitutive law adopted for DEM uni-axial elements.

dition that the energies dissipated by fracture of the continuum and by its discrete representation are equivalent. With this purpose, fracture of a cubic sample of dimensions $L \times L \times L$ is considered. The energy dissipated by fracture of a continuum cube due to a crack parallel to one of its faces is:

$$\Gamma = G_f \Lambda = G_f L^2 \quad (3)$$

in which Λ is the actual fractured area, *i.e.*, L^2 . On the other hand, the energy dissipated when a DEM module of dimensions $L \times L \times L$ fractures in two parts consists of the contributions of five longitudinal elements (four coincident with the module edges and an internal one) and four diagonal elements. Then, the energy dissipated by the DEM module can be written as follows (Kosteski *et al.*, 2010):

$$\Gamma_{DEM} = G_f \left(40.25c_a + c_a + 4c_a \left(\frac{2}{\sqrt{3}} \right)^2 \right) L^2 \quad (4)$$

The first term between brackets accounts for the four edge elements, the second term for the internal longitudinal element, while the third term represents the contribution of the four diagonal elements. The coefficient c_a is a scaling parameter used to establish the equivalence between Γ and Γ_{DEM} . Thus:

$$G_f L^2 = G_f \left(\frac{22}{3} c_a \right) L^2 \quad (5)$$

from which it follows that $c_a = 3/22$. Finally, the equivalent transverse fracture area of the longitudinal elements is:

$$A_l^* = \left(\frac{3}{22}\right)L^2 \tag{6}$$

while for the diagonal elements is:

$$A_d^* = \left(\frac{4}{22}\right)L^2 \tag{7}$$

These values apply as long as *there is a single large crack in the element*. The critical failure strain (ϵ_p) is defined as the largest strain attained by the element before the damage initiation (point A in Figure 3). The relationship between ϵ_p and the specific fracture energy G_f is given in terms of Linear Elastic Fracture Mechanics as:

$$\epsilon_p = R_f \sqrt{\frac{G_f}{E}} \tag{8}$$

in which R_f is the so-called failure factor, which may accounts for the presence of an intrinsic defect of size a . R_f may be expressed in terms of a as:

$$R_f = \frac{1}{Y\sqrt{a}} \tag{9}$$

in which Y is a dimensionless parameter that depends on both the specimen and crack geometry.

The element loses its load carrying capacity when the limit strain ϵ_r is reached (Point B in Figure 3). This value must satisfy the condition that, upon failure of the element, the dissipated energy density equals the product of the element fracture area A_i^* times the specific fracture energy G_f , divided by the element length. Hence:

$$\int_0^{\epsilon_r} F(\epsilon)d\epsilon = \frac{G_f A_i^*}{L_i} = \frac{K_r \epsilon_p^2 E A_i}{2} \tag{10}$$

in which the sub index i is replaced by l or d depending on whether the element under consideration is a longitudinal or diagonal. The coefficient K_r is a function of the material properties and the element length L_i :

$$K_r = \left(\frac{G_f}{\epsilon_p^2 E}\right) \left(\frac{A_i^*}{A_i}\right) \left(\frac{2}{L_i}\right) \tag{11}$$

In order to guarantee the stability of the algorithm, the condition $K_r \geq 1$ must be satisfied (Riera and Rocha, 1991). In this sense it is interesting to define the critical element length:

$$L_{cr} = 2 \left(\frac{G_f}{\varepsilon_p^2 E} \right) \left(\frac{A_i^*}{A_i} \right) \quad (12)$$

Moreover:

$$\left(\frac{A_l^*}{A_l} \right) = \left(\frac{3/22}{\phi} \right) \quad (13)$$

$$\left(\frac{A_d^*}{A_d} \right) = \left(\frac{\sqrt{3}/11}{\delta\phi} \right) \quad (14)$$

In the special case of an isotropic continuum with $\nu = 0.25$, the value of the coefficients above are $\delta = 1.125$ and $\phi = 0.4$, which leads to $(A_l^*/A_l) \approx (A_d^*/A_d) \approx 0.34$. Thus, for practical purposes, a single value of the critical length can be used for longitudinal and diagonal elements. Therefore, the stability condition may be expressed as:

$$K_r = \frac{L_{cr}}{L_i} \geq 1 \Rightarrow L_i \leq L_{cr} \quad (15)$$

Finally, the expression for the limit strain is:

$$\varepsilon_r = K_r \varepsilon_p \quad (16)$$

It is worth noting that although the DEM uses a scalar damage law to describe the uniaxial behavior of the elements, the global model accounts for anisotropic damage since it possess elements orientated in the different spatial directions. Miguel *et al.* (2008, 2010) and Iturrioz *et al.* (2009) modeled the random properties of material assuming the toughness G_f as a random field with a Type III (Weibull) extreme value distribution, given by:

$$F(G_f) = 1 - \exp[-(G_f/\beta)^\gamma] \quad (17)$$

in which β and γ are the scale and shape parameters, respectively. The mean value (μ) and the standard deviation (s) of G_f are given by:

$$\mu = \beta [\Gamma(1 + 1/\gamma)] \quad (18)$$

$$s = \beta [\Gamma(1 + 2/\gamma) - \Gamma^2(1 + 1/\gamma)]^{1/2} \quad (19)$$

in which $\Gamma(x) = \int_0^{\infty} t^{x-1} e^{-t} dt$ denotes the *Gamma* function.

In order to simulate pseudo random values of G_f the following expression was used:

$$G_f = \beta [-\ln(1 - u)]^{1/\gamma} \quad (20)$$

in which u is a random number with uniform probability distribution in the interval (0,1). Routines for generating samples of u are widely available. In earlier applications of the DEM, by taking the size of the elements (L_o) equal to the correlation length of the random field of the material property of interest, say l_c , allowed assuming that simulated values were uncorrelated, thus simplifying the computational scheme. This is however an important limitation of the model, initially addressed by Rios (2002). Later, Miguel (2005) adopted the method proposed by Shinozuka and Deodatis (1996) to simulate the gaussian 3D random field that represents the material property of interest. A simpler technique was employed by Puglia *et al.* (2010). This method was used herein to simulate the 3D random field that describes the toughness G_f , which is then independent of the discretization adopted in the DEM.

Thus, in the following analysis a DEM mesh is generated. Then, random values of the desired property are generated, according to the specified probability distribution function, at nodal points in a 3D grid with lengths (l_{cx} , l_{cy} , l_{cz}) in the three Cartesian directions. l_{cx} , l_{cy} and l_{cz} represent the correlation lengths of the random field in the x, y, z directions. The random values at the location of DEM elements are determined by a linear 3D interpolation from the values at the nodes. Additional details may be found in Puglia *et al.* (2010).

Applications of the method in studies involving non-homogeneous brittle materials subjected to fracture, like concrete and rock, may be found in Riera and Iturrioz (1998), Dalguer *et al.* (2003), Miguel *et al.* (2008), Iturrioz *et al.* (2009) and Miguel *et al.* (2010).

5 Analysis of cubic concrete samples subjected to high strain rates tension

Concrete cubic samples fixed at the lower face and subjected to increasing uniformly distributed prescribed displacements on the upper face inducing in the sample nominal uniform tension were analyzed with different loading rates. The response of each test up to failure was determined through numerical simulation. The samples were analyzed under increasing controlled displacements on the up-

per face with different (constant) rates, maintaining all other features unaltered, inducing nominal tensile stresses.

Sample dimensions were $0.15 \times 0.15 \times 0.15$ m, while the mesh employed in all simulations included $15 \times 15 \times 15$ DEM cubic modules, implying that $L_o = 0.010$ m. In the ensuing simulations, the specific fracture energy was assumed to be a 3D random field with $\mu(G_f) = 90$ N/m, and $CV(G_f) = 0.5$, while Young's modulus $E = 3.5E10$ N/m², Poisson's ratio $\nu = 0.25$ and specific mass $\rho = 2400$ kg/m³ were considered constant.

Reaction force-displacement curves for various rates in simulated displacement controlled tests are shown in Figure 4. Note that the dot line, corresponding to the fastest rate, presents anomalies due to wave propagation effects. A strength increase is observed when the loading rate increases, which is in agreement with the experimental results presented in Figure 1. Notice that for a specimen length equal to 0.15 m, the applied velocities ($8e-2$ m/s, $3e-2$ m/s and $5e-4$ m/s) are equivalent to the strain rates (0.53 /s, 0.20 /s and $3.33e-3$ /s). A typical crack pattern at a central slice of the sample is shown in Figure 5, in which the boundary conditions are also indicated.

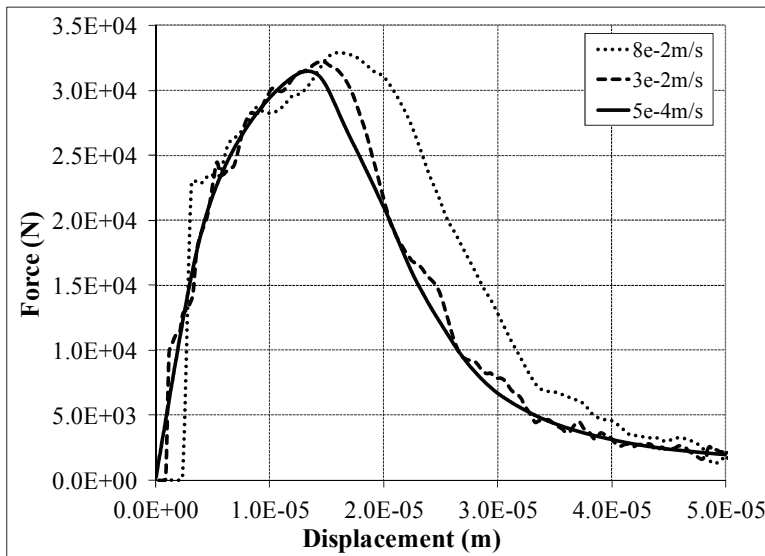


Figure 4: Numerical DEM simulations of the tensile force on the lower face vs. applied displacement for same concrete specimen subjected to three loading rates.

A single function for the ratio η between the dynamic and the static strengths, based on the assumption that linear relations are valid for low and high strain rates,

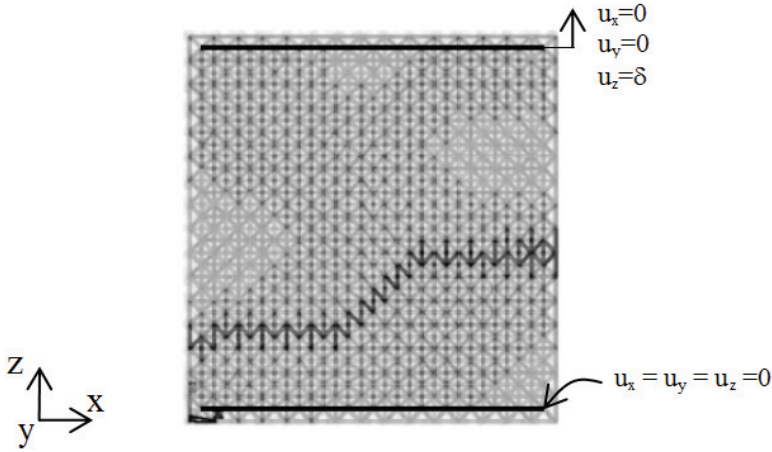


Figure 5: Typical rupture configuration in a DEM simulation (undamaged elements are shown in light grey, damaged elements in dark gray and failed elements in black).

but that there is a smooth transition, modeled by the logistic distribution $f(x)$, in which $x = \log(\dot{\epsilon})$, was fitted to the simulated results (Miguel *et al.*, 2012):

$$\eta(x) = (a_1 + b_1x) f(x) + (a_2 + b_2x) [1 - f(x)] \quad (21)$$

$$f(x) = \exp[-(x + x_c)/s] / \{1 + \exp[-(x + x_c)/s]\} \quad (22)$$

Taking the logarithm x_c of the transition strain rate $\dot{\epsilon}_c$ equal to 0.1 and the coefficient s equal to 0.1, the following parameters were calculated by means of a regression analysis: $a_1 = 1.71$, $b_1 = 0.13$, $a_2 = 2.24$ and $b_2 = 2.25$. Equation (21) is plotted as a blue curve in Figure 2 and is apparently compatible with the experimental evidence. However, it must be mentioned that physical or numerically simulated displacement controlled tensile tests are valid only if the ratio between the applied displacement rate a and the P -wave velocity c_p in the material does not exceed the strain ϵ_{min} at which damage begins to occur in the material. Thus, consider for instance a cylindrical bar of area A and length L fixed at the end $x = 0$ and subjected at the opposite end $x = L$ to a linearly increasing displacement $u = at$ that induces uniaxial tension in the x -direction in the bar. If the rate of loading, defined by coefficient a (m/s), is very small, a quasi-static response may be expected, in which

case the axial strain at any time t would be given by the simple expression:

$$\varepsilon = at/L \quad (23)$$

Moreover, in such case the reaction F_x at the fixed support will be given by:

$$F_x = \varepsilon E = aEt/L \quad (24)$$

The strain ε would be constant throughout the length of the bar. However, as the rate of loading a increases, equations (23) and (24) are no longer applicable, since when dynamic effects appear, ε and consequently the axial force on the bar become functions of both x and t , while the support reaction F_x will vary with t , but *cannot be correlated with a generic or average axial strain*. It is thus clear that the plots of the relation between F_x and the average strain ε_{av} presented in the technical literature are truly meaningful for small loading rates but become questionable at intermediate rates and totally meaningless for very high loading rates. Denoting the velocity of propagation of pressure waves in the material (P waves) as c_p , which is approximately given by:

$$c_p = (E/\rho)^{1/2} \quad (25)$$

in which E denotes Young's modulus and ρ the specific mass of the material, if the excitation $u = at$ starts at $t = 0$, the peak strain within the loaded zone - whose length is $c_p t$ - *cannot be smaller than*:

$$\varepsilon_{\min} = at/c_p t = a/c_p \quad (26)$$

Thus, equation (26) provides a lower limit for the maximum axial strain in the loaded region of the bar. It is then concluded that direct tensile loading of the sample is not feasible or at least questionable when:

$$\varepsilon_{\min} > \varepsilon_p \quad (27)$$

in which ε_p denotes the axial strain at which damage begins to occur in the material. This explains why the simulations for very high strain rates yielded absurd results and suggests a limit strain rate for which the simulations may be accepted. Substituting typical expected values for c_p and ε_p for concrete in equations (26) and (27) above, an upper limit of around $1/s$ results for the strain rate in direct tensile tests. Due to the heterogeneous nature of concrete, which should result in more complex features of the wave propagation field than assumed in the preceding analysis, this limit is regarded as merely indicative of the range of validity of equation (21).

6 Analysis of modified Hopkinson's bar tensile tests

In order to examine further the performance of DEM models in predicting tensile failure under high strain rates, the authors analyzed the tests described by Hentz *et al.* (2004) and Brara and Klepaczko (2007). Initially used in compression, the SHPB technique was later extended to tension. In this scheme there is only one input bar and no output bar, as schematically shown in Figure 6. A projectile impacts the input bar, giving rise to a compressive wave, which propagates into the specimen and reflects as a tensile wave at its free end. If the wavelength of the loading pulse is longer than the specimen length, the reflected tensile wave is superposed to its own back tail still propagating.

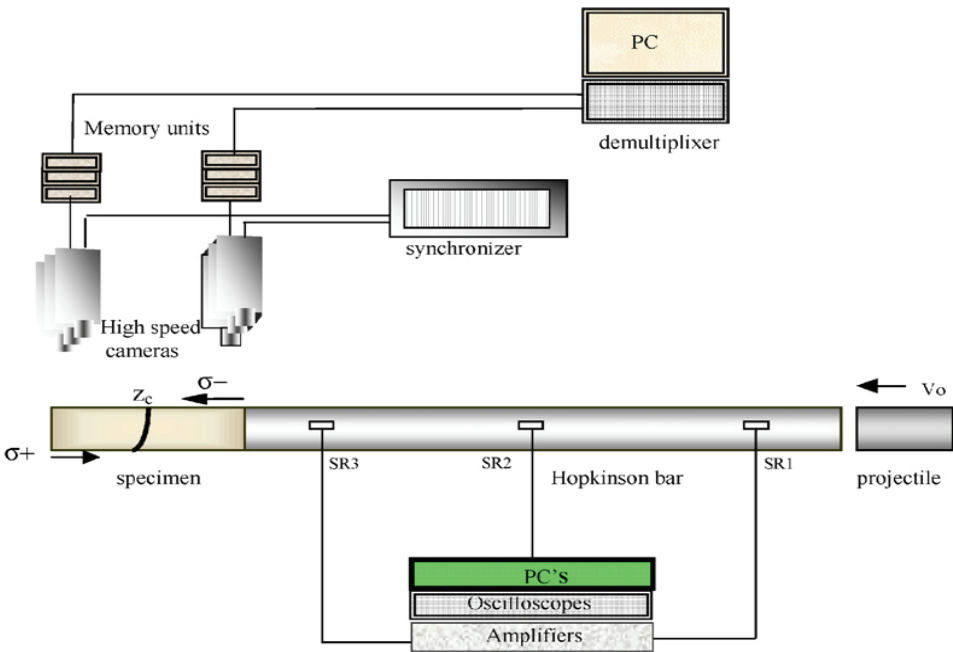


Figure 6: Experimental set-up of the split Hopkinson bar (from Brara and Klepaczko, 2007).

Addition of the two parts of the pulse gives rise to tensile stresses in the specimen, leading to complete rupture if its amplitude is sufficiently high. The concrete properties in the experimental program had the following quasi-static properties: Young's modulus $E = 35\text{GPa}$, mass density $\rho = 2400\text{kg/m}^3$, compressive strength $f_c = 42\text{MPa}$ and tensile strength $f_t = 4\text{MPa}$. The samples were 120mm long circular cylinders with 40mm diameter (Hentz *et al.*, 2004). In the following, simulated

results for prismatic samples with the same length and 40mm side length square base will be presented.

The samples were subjected to the impulsive load shown in Figure 7 for a 50kN amplitude, which is a very close approximation to the load measured in the tests. The shapes and durations of the load diagrams for the amplitudes analyzed in this paper, namely 20, 40 and 80kN were assumed to be the same. Moreover, as previously discussed, the specific fracture energy is assumed a 3D random field, for which three samples, denoted samples 1, 2 and 3, were simulated. Each sample was then subjected to the three impulsive load functions considered in the study. Of course, *in the laboratory the same physical specimen cannot be subjected to different impulsive loadings*. This will be an important consideration in the assessment of the results.

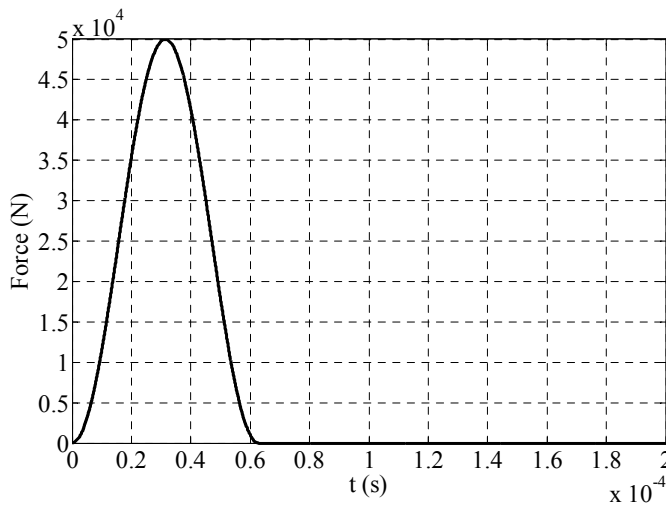


Figure 7: Force vs. time diagram of impulsive load applied as uniform pressure on left face of specimen. In the various numerical simulations herein reported only the 50kN amplitude varies.

Figure 8 shows a plot of the mean stress vs. time at the center cross-section ($x = 0.06\text{m}$) of the specimen (sample 1) for three impulsive load amplitudes (20, 40 and 80kN, which are equivalent to the peak strain rates: 17.8/s, 34.6/s and 64.8/s). It may be seen that the compressive pulse amplitudes, which occur shortly before 0.05ms, increase more or less linearly with the loading pulse amplitudes, while the returning tensile wave *is limited* by the assumed constitutive relation. It should be underlined that *stresses cannot be measured*, since only kinematic variables are susceptible of direct observation.

Figure 9 shows the corresponding mean axial strain vs. time curves, also for sample 1 and the three load functions. It may be clearly seen that while for load amplitudes 20 and 40kN the sample presents limited damage at the cross-section under consideration, it has already failed for the largest amplitude 80kN.

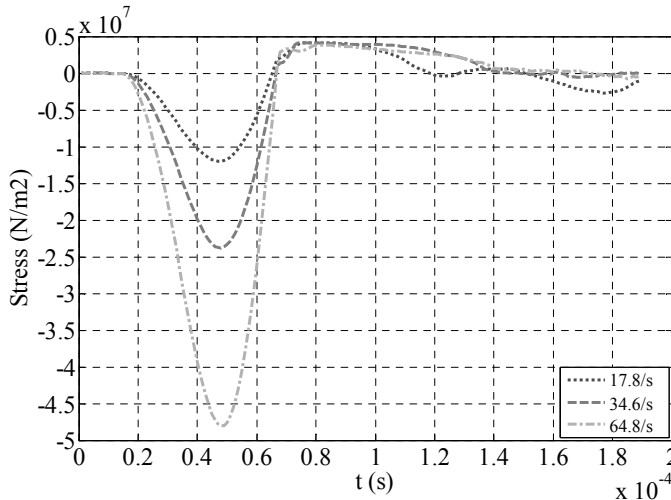


Figure 8: Plot of the mean stress vs. time at the center cross-section ($x = 0.06\text{m}$) of the specimen (sample 1) for three impulsive load amplitudes (20, 40 and 80kN).

One relevant factor, that is mentioned neither in experimental nor in numerical studies, is brought to light by Figure 10, which presents the strain rate vs. time curves at the central cross-section ($x = 0.06\text{m}$) of the specimen (sample 1). Since most reports in the literature indicate values of the tensile strength *for given strain rates*, the question about which rate is being referred to seems pertinent. In this paper the authors will use as reference the *peak value of the rate vs. time curve*, but suggest that the criterion should be restrained to cases in which the rate vs. time curve does not present pronounced spikes.

Stress vs. strain diagrams may be obtained from Figures 8 and 9. Figure 11, for instance, shows plots of the mean stress vs. mean strain at the central cross-section ($x = 0.06\text{m}$) of the specimen (sample 1) for three impulsive load amplitudes (20, 40 and 80kN). It may be seen that for the 20kN amplitude in sample 1, there is a closed hysteresis cycle at ($x = 0.06\text{m}$). Perceptible damage occurs for the 40kN load amplitude, but the cycle is still closed, while for 80kN the strain tends to increase indefinitely.

A plot of the axial experimental stress vs. strain curve in specimen tested in a Hop-

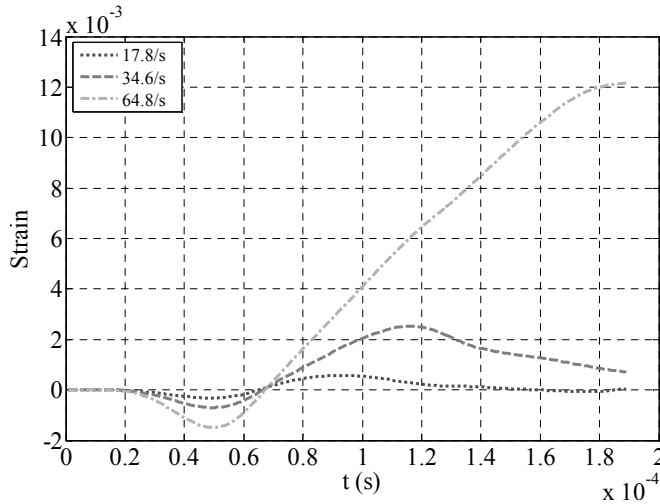


Figure 9: Plot of the mean strain vs. time at the center cross-section ($x = 0.06\text{m}$) of the specimen (sample 1) for three impulsive load amplitudes (20, 40 and 80kN).

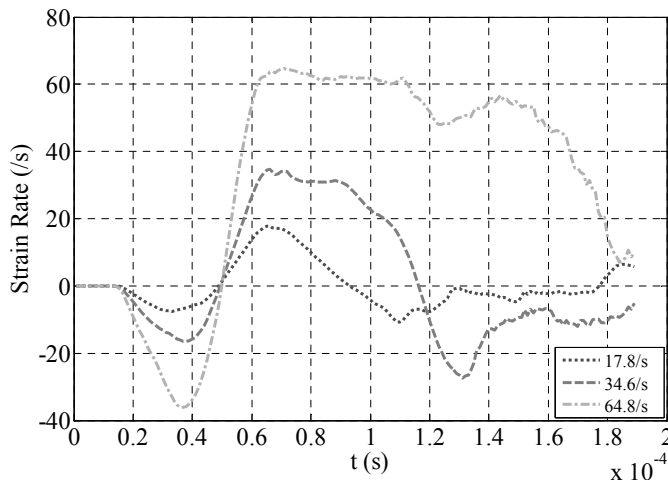


Figure 10: Plot of the axial strain rate vs. time at the center cross-section ($x = 0.06\text{m}$) of the specimen (sample 1) for three impulsive load amplitudes (20, 40 and 80kN).

kinson bar by Weerheijm and Van Doormaal (2007), showing a striking similarity with one of the cycles (for 40kN) in Figure 11 is presented in Figure 12.

Figure 13 presents the distribution of the axial strain along the centerline of the

specimen for the three load amplitudes, again for sample 1. It is clear that for a load amplitude of 20kN, a single large fracture tends to develop at $x \sim 0.40\text{m}$, splitting the sample in two parts. For a load of 40kN a second fracture is detected at $x \sim 0.53\text{m}$ while in the third case the specimen is split in several parts.

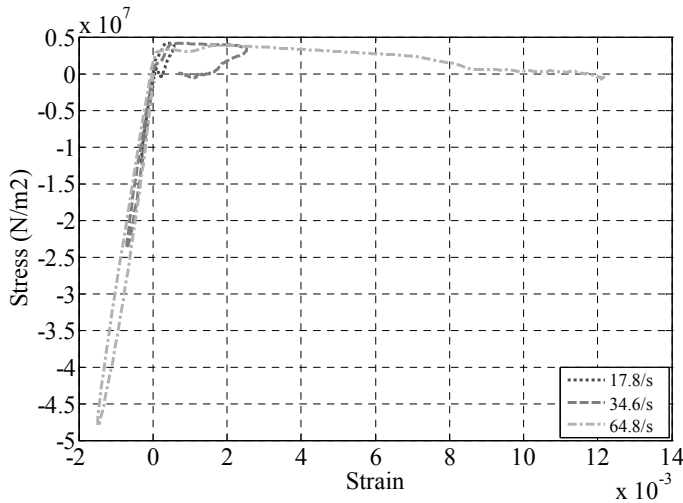


Figure 11: Plot of the mean stress vs. mean strain at the center cross-section ($x = 0.06\text{m}$) of the specimen (sample 1) for three impulsive load amplitudes (20, 40 and 80kN).

Finally, Figure 14 shows the rupture configurations for the three impulsive loads considered in the study, with amplitudes equal to 20, 40, and 80kN, respectively, and for the three simulated samples. Undamaged DEM elements were identified in black, damaged elements in grey and broken (failed) elements in white. Thus, dark color indicates undamaged or slightly damaged and light grey highly damaged regions. Fractures can be seen as white bands.

Note that for low amplitude load pulses (20 and 40kN) fractures occur close to $x = 0.40\text{m}$ in samples 1 and 3, which are similar to the configuration obtained by Hentz *et al.* (2004) for a 50kN amplitude (see Figure 15). This may be a preferred location for load amplitudes below 50kN, but it should be acknowledged that the first fracture may take place at a weak section elsewhere. This is illustrated by the rupture configurations of sample 2, which presents a large, clearly defined fracture close to $x \sim 0.80\text{m}$ for all loading cases. It was verified that for an input load amplitude equal to 80kN, the sample splits in several parts (Figure 14), ranging from three to six or so, depending on the distribution of the fracture energy. This result also coincides with experimental observations. However, the average tensile

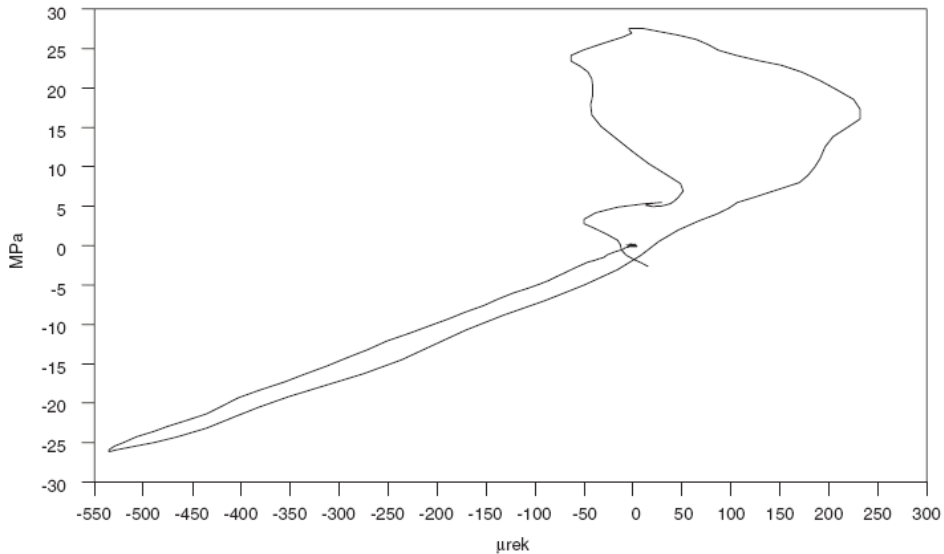


Figure 12: Plot of axial experimental stress *vs.* strain in specimen tested in a Hopkinson bar by Weerheijm and Van Doormaal (2007), showing similarity with one of the cycles in Figure 11.

stress at a sample cross-section at mid-length never exceeds around 5MPa, as may be seen in the typical mean stress *vs.* time plot shown in Figure 8, which casts doubts on the large increase in both the tensile strength and the specific fracture energy reported for high strain rates by Hentz *et al.* (2004) and others.

In fact, the increase in the tensile strength as the strain rate increases observed in engineering experiments seems to be due, for strain rates below 1/s, to the increase of micro-cracks resulting from the dynamic loading and the ensuing increase in fracture energy. The authors see no reason to expect a much larger increase of the strength for higher strain rates and sustain that, until further evidence is available, the specific fracture energy of concrete should not be significantly increased for the analysis of structures subjected to impact or explosive loadings.

7 Conclusions

The authors have extensively employed the truss-like Discrete Element Method (DEM) described in the paper, to predict the response of concrete structures subjected to impulsive and impact loading. In cases in which failure *is caused primarily by tensile stresses*, as in punching-through of plate or shell structures, the

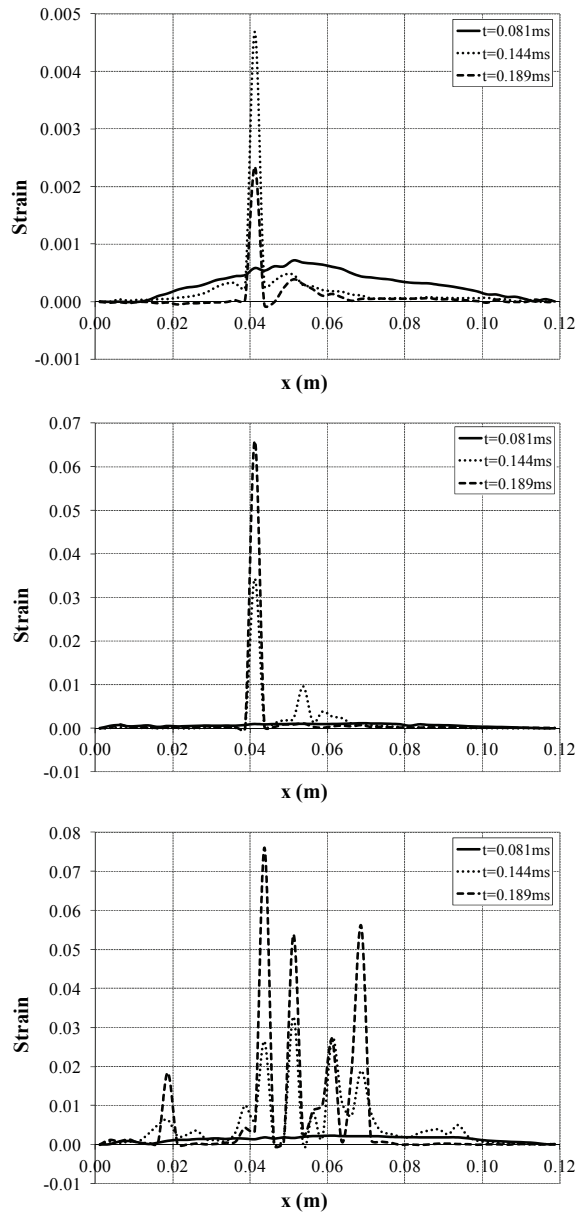


Figure 13: Plots of the axial nominal strain at the center ($y = z = 0$) of the specimen vs. x -coordinate for impulsive load amplitudes of 20 (above), 40 (center) and 80kN (below), respectively, showing the locations of transverse fractures in sample 1. Spikes of the strain plots actually indicate cracks.

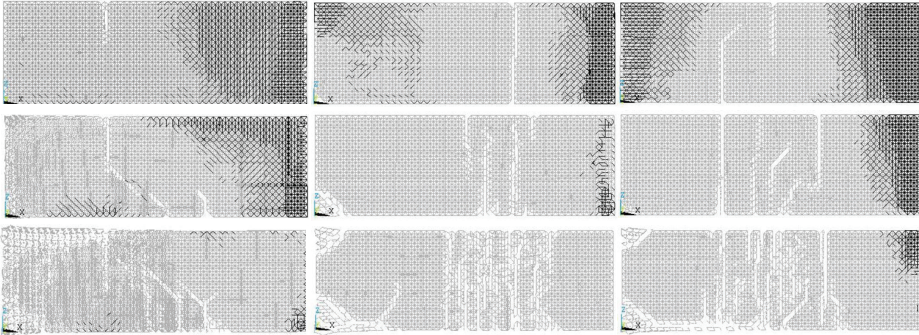


Figure 14: DEM predictions of the rupture configurations at $t = 1.89 \times 10^{-4}$ s for impulsive loads amplitudes of 20kN (above), 40kN (center line) and 80kN (below), for simulated sample 1 (left), sample 2 (center column) and sample 3 (right).

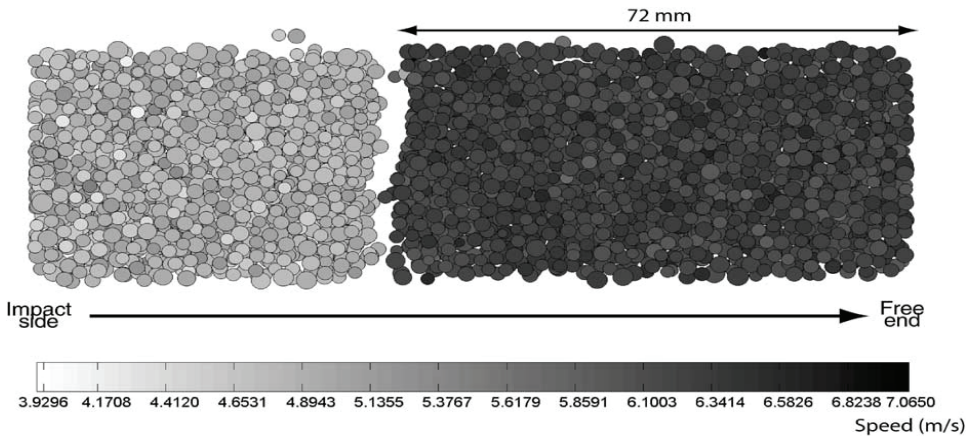


Figure 15: View of Hentz *et al.* (2004) numerical prediction of the fracture configuration for BE16 test with the modified model: Axial speed field in the specimen at $t = 3.28 \times 10^{-3}$ s.

basic constitutive law suggested by Hillerborg used herein in conjunction with consideration of the heterogeneous character of concrete, has shown to be both robust and reliable, in terms of small prediction errors when compared with experimental results.

One initially surprising prediction of simulation studies was the detection of *strain rate effects*, that is, the *computed* strength of structural elements was observed to increase as the loading or strain rates increased, *without any change in the consti-*

tutive equations or material parameters. Initial studies were then aimed at determining the response of cubic samples subjected to controlled displacements, which confirmed the capacity of the DEM to predict the experimentally observed strength increase with the strain rate in tensile tests. However, it is shown that this approach, both in laboratory and in numerical simulation studies of concrete, is limited to strain rates smaller than about 1/s.

Hence, modified split Hopkinson bar published test results were simulated, employing the present DEM formulation, which was able to reproduce the observed failure configurations, but in contradictions with published results in the technical literature, do not predict *large* tensile strength or specific fracture energy increases with the strain rate. In fact, since it is not possible to directly measure the transient dynamic stresses in the tested samples, the correctness of proposed models can only be confirmed by comparisons of simulation results with the experimental damage configurations. As far as the authors are aware of, in none of the available Hopkinson bar experimental studies it was attempted to determine damage in the remaining parts of the split samples, which is essential to correctly predict the response.

Acknowledgement: The authors acknowledge the support of CNPq and CAPES (Brazil).

References

Brara, A., Camborde, F., Klepaczko, J. R. and C. Mariotti, C., (2001). Experimental and numerical study of concrete at high strain rates in tension, *Mechanics of Materials*, 33, 33-45.

Brara, A. and Klepaczko, J. R., (2007). Fracture energy of concrete at high loading rates in tension, *International Journal of Impact Engineering*, 34, 424–435.

Cotsovos, D. M. and Pavlovic', M. N., (2008). Numerical investigation of concrete subjected to high rates of uniaxial tensile loading, *International Journal of Impact Engineering*, 35, 319–335.

Dalguer, L. A., Irikura, K., and Riera, J. D., (2003). Simulation of tensile crack generation by three-dimensional dynamic shear rupture propagation during an earthquake. *J. Geophys. Res.*, 108(B3), 2144.

Hentz, S., Donzé, F. V. and Daudeville, L., (2004). Discrete element modelling of concrete submitted to dynamic loading at high strain rates, *Computers and Structures*, 82, 2509–2524.

Hillerborg, A., (1971). A model for fracture analysis, Cod. LUTVDG/TVBM

300-51-8.

Iturrioz, I., Miguel, L. F. F., and Riera, J. D., (2009). Dynamic fracture analysis of concrete or rock plates by means of the Discrete Element Method. *Latin American Journal of Solids and Structures*, Vol. 6, pp. 229-245.

Kim, K. and Lim, Y. M., (2011). Simulation of rate dependent fracture of concrete using an irregular lattice model, *Cement and Concrete Composites*, doi: 10.1016/cemconcomp.2011.01-002.

Kosteski, L. E., Riera, J. D. and Iturrioz, I. (2010). Consideration of scale effects and stress localization in response determination using the DEM, *MECOM – CILAMCE 2010*, November 2010, Buenos Aires, Argentina.

Malvar, I. J. and Crawford, J. E., (1998). Dynamic increase factors for concrete, *28th Department of Defense Explosive Safety Seminar*, Orlando, Florida, USA.

Miguel, L. F. F. (2005). Critério constitutivo para o deslizamento com atrito ao longo da falha sísmica, *Ph.D. thesis*, (in portuguese) 229 pp., PPGEC, Escola de Engenharia, Universidade Federal do Rio Grande do Sul, Porto Alegre, Brazil.

Miguel, L. F. F., Riera, J. D., and Iturrioz, I., (2008). Influence of size on the constitutive equations of concrete or rock dowels. *International Journal for Numerical and Analytical Methods in Geomechanics*, Vol. 32, No. 15, pp. 1857-188, doi: 10.1002/nag.699.

Miguel, L. F. F., Iturrioz, I., and Riera, J. D., (2010). Size Effects and Mesh Independence in Dynamic Fracture Analysis of Brittle Materials, *CMES: Computer Modeling in Engineering & Sciences*, 56, pp. 1-16.

Miguel, L. F. F., Riera, J. D., and Iturrioz, I., (2012). Rate effects in brittle materials subjected to tension. *Proceedings of PACAM XII - 12th Pan-American Congress of Applied Mechanics*, January 02-06, 2012, Port of Spain, Trinidad.

Ozbolt, J., Sharma, A. and Reinhardt, H-W., (2011). Dynamic fracture of concrete compact tension specimen, *International J. of Solids and Structures*, 48, 1534-1543.

Puglia, V. B., Iturrioz, I., Riera, J. D., Kosteski, L. E., (2010). Random field generation of the material properties in the truss-like discrete element method, *Mecánica Computacional, Cilamce-Mecom 2010*, v. XXIX, pp 6793-6807.

Riera, J. D. (1984). Local effects in impact problems on concrete structures. *Proceedings, Conference on Structural Analysis and Design of Nuclear Power Plants*, Oct. 1984, Porto Alegre, RS, Brasil, Vol. 3, CDU 264.04:621.311.2:621.039.

Riera, J. D. and Rocha, M. M., (1991). A note on the velocity of crack propagation in tensile rupture, *Revista Brasileira de Ciências Mecânicas - RBCM*, VII (3), 217-240.

Riera, J. D. and Iturrioz, I., (1998). Discrete elements model for evaluating impact and impulsive response of reinforced concrete plates and shells subjected to impulsive loading. *Nuclear Engineering and Design*, 179, 135-144.

Riera, J. D.; Iturrioz, I.; and Miguel, L. F. F., (2008). On Mesh Independence in Dynamic Fracture Analysis by Means of the Discrete Element Method. *ENIEF 2008 - XVII Congreso sobre Métodos Numéricos y sus Aplicaciones*, San Luis, Argentina, 2008. v. XXVII. p. 2085-2097.

Rios, R. D. (2002). Aplicações do método dos elementos discretos em estruturas de concreto, *Ph.D. thesis*, PPGEC, Universidade Federal do Rio Grande do Sul, Porto Alegre, Brazil.

Rios, R. D., and Riera, J. D., (2004). Size effects in the analysis of reinforced concrete structures. *Engineering Structures*, Vol 26, Issue 8, 1115-1125.

Shinozuka, M. and Deodatis, G., (1996). Simulation of multi-dimensional gaussian stochastic fields by spectral representation, *Applied Mechanics Review*, American Society of Mechanical Engineers, 49(1), 29-53.

Van Vliet, M. R. A. and Van Mier, J. G. M., (2000). Size effects of concrete and sandstone, *Heron*, Vol 45, No.2, 91-108.

Weerheijm, J. and Van Doormaal, J. C. A. M., (2007). Tensile failure of concrete at high loading rates: New test data on strength and fracture energy from instrumented spalling tests, *International Journal of Impact Engineering*, 34, 609–626.